Design of Reversible Low-Field Magnetocaloric Effect at Room Temperature in Hexagonal MnMX Ferromagnets

Liu, Jun; You, Yurong; Batashev, Ivan; Gong, Yuanyuan; You, Xinmin; Huang, Bowei; Zhang, Fengqi; Miao, Xuefei; Xu, Feng; Van Dijk, Niels

DOI
10.1103/PhysRevApplied.13.054003

Publication date
2020

Document Version
Final published version

Published in
Physical Review Applied

Design of Reversible Low-Field Magnetocaloric Effect at Room Temperature in Hexagonal Mn*MX* Ferromagnets

Jun Liu,[1,2,*] Yurong You,[2] Ivan Batashev,[1] Yuanyuan Gong,[2] Xinmin You,[1] Bowei Huang,[1] Fengqi Zhang,[1] Xuefei Miao,[2] Feng Xu,[2,†] Niels van Dijk,[1] and Ekkes Brück[1]

[1] *Fundamental Aspects of Materials and Energy (FAME), Faculty of Applied Sciences, Delft University of Technology, Mekelweg 15, 2629 JB Delft, Netherlands*

[2] *MIIT Key Laboratory of Advanced Metallic and Intermetallic Materials Technology, School of Materials Science and Engineering, Nanjing University of Science and Technology, Nanjing 210094, China*

(Received 15 December 2019; revised manuscript received 10 March 2020; accepted 7 April 2020; published 1 May 2020)

The giant magnetocaloric effect is widely achieved in hexagonal Mn*MX*-based (M = Co or Ni, X = Si or Ge) ferromagnets at their first-order magnetostructural transition. However, the thermal hysteresis and low sensitivity of the magnetostructural transition to the magnetic field inevitably lead to a sizeable irreversibility of the low-field magnetocaloric effect. Here, we show an alternative way to realize a reversible low-field magnetocaloric effect in Mn*MX*-based alloys by taking advantage of the second-order phase transition. With introducing Cu into Co in stoichiometric MnCoGe alloy, the martensitic transition is stabilized at high temperature, while the Curie temperature of the orthorhombic phase is reduced to room temperature. As a result, a second-order magnetic transition with a negligible thermal hysteresis and a large magnetization change can be observed, enabling a reversible magnetocaloric effect. By both calorimetric and direct measurements, a reversible adiabatic temperature change of about 1 K is obtained under a field change of 0–1 T at 304 K, which is larger than that obtained in a first-order magnetostructural transition. To gain a better insight into the origin of these experimental results, first-principles calculations are carried out to characterize the chemical bonds and the magnetic exchange interaction. Our work provides an understanding of the MnCoGe alloy and indicates a feasible route to improve the reversibility of the low-field magnetocaloric effect in the Mn*MX* system.

DOI: 10.1103/PhysRevApplied.13.054003

I. INTRODUCTION

A strong coupling between a first-order structural change and a magnetic phase transition, the so-called magnetostructural transition (MST), can bring about a giant magnetocaloric effect (MCE) [1–4]. Magnetic refrigeration (MR) based on the MCE is environmentally friendly and highly energy efficient, and is therefore considered to be promising technology to replace conventional gas refrigeration [5,6]. As one of the candidate materials for MR at room temperature, the hexagonal Mn*MX*-based (M = Co or Ni, X = Si or Ge) ferromagnets, which experience a martensitic transition, attract much attention, owing to significant advantages: (i) a strong magnetostructural coupling can easily be established and be highly tuned between the Curie temperatures of two phases by elemental substitution [7–9], the introduction of vacancies [10,11], and hydrostatic pressure [12,13]; (ii) the featured paramagnetic-ferromagnetic- (PM-FM) type MST gives rise to the same sign of enthalpy change during the martensitic and magnetic transitions, leading to a higher magnetic entropy change ($|\Delta S_m|$) than that of other magnetocaloric materials [8,14,15]; and (iii) compounds with desired compositions can be produced easily.

Nevertheless, the first two points, in turn, bring about evident disadvantages to Mn*MX*-based system. First, the first-order nature of the MST inevitably results in the occurrence of thermal and magnetic hysteresis. Second, according to the Clausius-Clapeyron equation, the giant entropy change greatly decreases the sensitivity of structural transition temperature (T_t) to the magnetic stimulus [12,16]. Both drawbacks result in a significant functional fatigue of the giant MCE in magnetic cycles [17]. Our previous work showed that a giant reversible $|\Delta S_m|$ ($>$20 J kg^{-1} K^{-1}) under the field change of 0–5 T could be obtained by minimizing the thermal hysteresis in the $Mn_{0.9}Fe_{0.2}Ni_{0.9}Ge_{1-x}Si_x$ system [18]. This sizeable reversibility of the MCE would significantly degrade for a low-field variation [18]. In addition, Liu *et al.* measured the adiabatic temperature change (ΔT_{ad}) during the MST in $MnCo_{0.95}Ge_{0.97}$, with a reversible value of only about

*liujun@njust.edu.cn
†xufeng@njust.edu.cn

0.7 K under a field change of 1.9 T [19]. Constructing an active magnetic refrigerator is desirable to operate under a cyclic low magnetic field change of 1 T at ambient temperature [20,21]. Under this cyclic field, the magnetic-field-induced MST is irreversible and the associated MCE is reduced, which directly hinders the potential for application of the Mn*MX* system as a magnetic coolant. Thus, it is of key importance to realize a reversible low-field (0–1 T) MCE at room temperature in Mn*MX* alloys.

Considering the intrinsic disadvantages of MST, we alternatively focus on the second-order phase transition (SOMT) in Mn*MX* alloy. Despite the moderate MCE of the SOMT, its transition is continuous, which may provide a feasible alternative to optimize the Mn*MX* system. Figure 1 shows the main design schematic. Here, we choose stoichiometric MnCoGe as the host material due to its large saturation magnetic moment (4.13 μ_B/f.u.) and magnetic transition near room temperature [22,23]. To realize our aim, two criteria should be met: (i) the martensitic transition needs to remain in the high-temperature range to lower its impact on the magnetic transition; and (ii) the Curie temperature of the orthorhombic phase (T_C^O) with higher magnetization should be tuned to room temperature. Here, we introduce Cu onto the Co site of stoichiometric MnCoGe to fulfill these goals. For an increasing Cu content, the martensitic transition temperature varies slightly and lies in the PM region. Simultaneously,

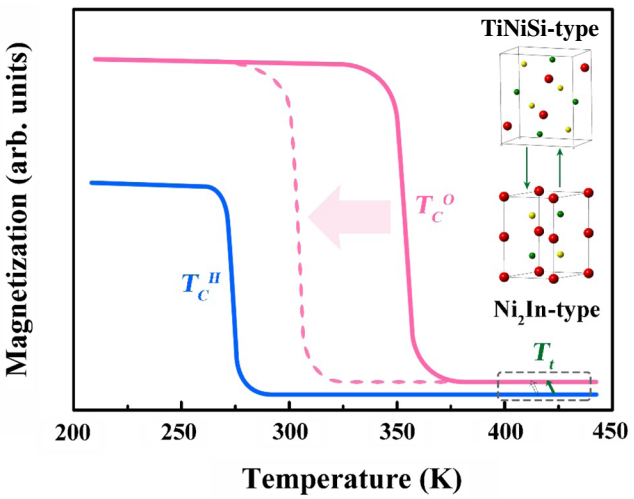

FIG. 1. Schematic of the alloy design for a room-temperature SOMT. Solid pink and blue curves are thermomagnetic curves of orthorhombic and hexagonal phases in the MnCoGe alloy, respectively. Solid green arrow represents the martensitic transition. As indicated by the dashed pink curve and dashed green arrow, T_C^O is aimed to be reduced to room temperature and the structural transition is stabilized in the high-temperature PM region (gray dashed box). Ni_2In-type and TiNiSi-type crystalline structures are also shown.

T_C^O is reduced to room temperature. Indirect (calorimetric) and direct measurements are adopted to evaluate the MCE performance of the $MnCo_{1-x}Cu_xGe$ system, in which tunable and reversible ΔT_{ad} and ΔS_m are achieved. In addition, the obtained experimental results are compared with first-principles calculations to unravel the possible physical mechanism of the evolution of the structural and magnetic transition behavior.

II. EXPERIMENTAL DETAILS AND CALCULATION METHOD

Polycrystalline samples with nominal compositions $MnCo_{1-x}Cu_xGe$ ($x = 0.00$, 0.06, 0.07, and 0.08) are prepared by arc-melting high-purity raw materials four times to ensure homogeneity. Then ingots sealed in vacuum quartz tubes are annealed at 1123 K for 5 days and slowly cooled to room temperature in 18 h. The thermal properties are measured in a differential scanning calorimeter (DSC, TA Instrument Q2000) with a heating and cooling rate of 10 K/min. The magnetic properties are measured on a superconducting quantum interference device (SQUID, Quantum Design MPMS 5XL) with the reciprocating sample option mode. The crystal structures are characterized by using a powder X-ray diffractometer at room temperature (XRD, PANalytical X'Pert PRO). The structural parameters are refined using the FullProf package [24]. The calorimetric measurements in applied magnetic field are carried out in a home-built DSC with a Pieter cell (details described in Ref. [25]), from which ΔS_m and ΔT_{ad} can be calculated. A direct ΔT_{ad} measurement device is employed to measure ΔT_{ad} under cyclic fields of 1.1 T

TABLE I. Lattice parameters, unit-cell volume, site occupation, goodness of the Rietveld refinement (R_{WP}), T_C^O, and ΔT_{ad} under a field change of 0–1 T for $MnCo_{1-x}Cu_xGe$ ($x = 0.00$, 0.06, 0.07, and 0.08). All atoms occupy Wyckoff position 4*c* (x, 1/4, z) in the orthorhombic phase. Due to restriction of the measurement temperature range, ΔT_{ad} for the sample with $x = 0.00$ cannot be obtained.

Sample	$x = 0.00$	$x = 0.06$	$x = 0.07$	$x = 0.08$
a (Å)	5.9643(2)	5.9993(1)	6.0131(2)	6.0195(1)
b (Å)	3.8211(1)	3.8153(1)	3.8146(1)	3.8136(1)
c (Å)	7.0597(2)	7.0607(1)	7.0638(2)	7.0634(2)
V (Å^3)	160.89(1)	161.61(1)	162.03(1)	162.14(1)
x_{Mn}	0.0301(7)	0.0259(7)	0.0414(8)	0.0225(7)
z_{Mn}	0.6898(5)	0.6848(4)	0.6905(5)	0.6865(4)
x_{Co-Cu}	0.1562(7)	0.1594(6)	0.1528(8)	0.1565(6)
z_{Co-Cu}	0.0569(5)	0.0594(4)	0.0590(6)	0.0561(5)
x_{Ge}	0.2702(5)	0.2685(5)	0.2657(6)	0.2660(5)
z_{Ge}	0.3817(4)	0.3748(3)	0.3821(5)	0.3770(3)
R_{WP} (%)	2.99	2.95	4.09	2.81
T_C^O (K)	348.9	314.0	305.9	295.9
ΔT_{ad} (K)	–	1.1	1.0	1.0

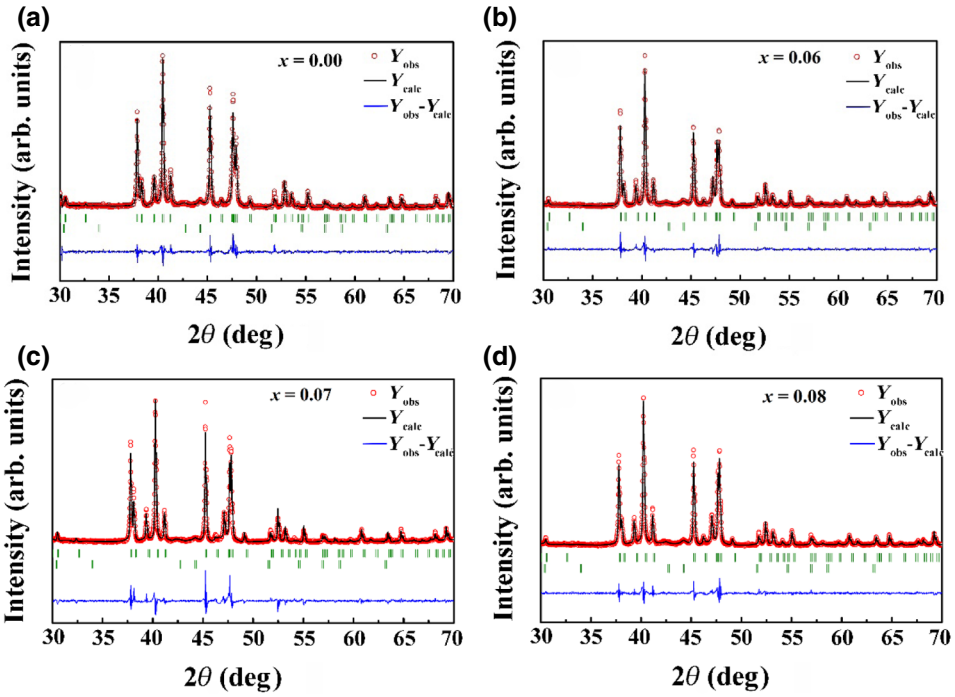

FIG. 2. XRD patterns at room temperature with the corresponding Rietveld refinements for $MnCo_{1-x}Cu_xGe$: (a) $x = 0.00$, (b) $x = 0.06$, (c) $x = 0.07$, and (d) $x = 0.08$.

at a rate of 1.1 T/s, as described in Ref. [26]. Here, the powder sample is compressed into a capsule and then a thermocouple is buried to guarantee good thermal contact.

Electronic localized function (ELF) calculations on the basis of density function theory was performed using the Vienna *ab initio* simulation package (VASP) [27]. We implement Perdew-Burke-Ernzerhof (PBE) pseudopotentials with generalized gradient approximation (GGA) exchange correlation functions. A plane-wave cutoff energy of 500 eV and $9 \times 9 \times 9$ **k** points are chosen. Here, a supercell of eight unit cells, with a hexagonal lattice structure, are considered. Geometry optimizations for the

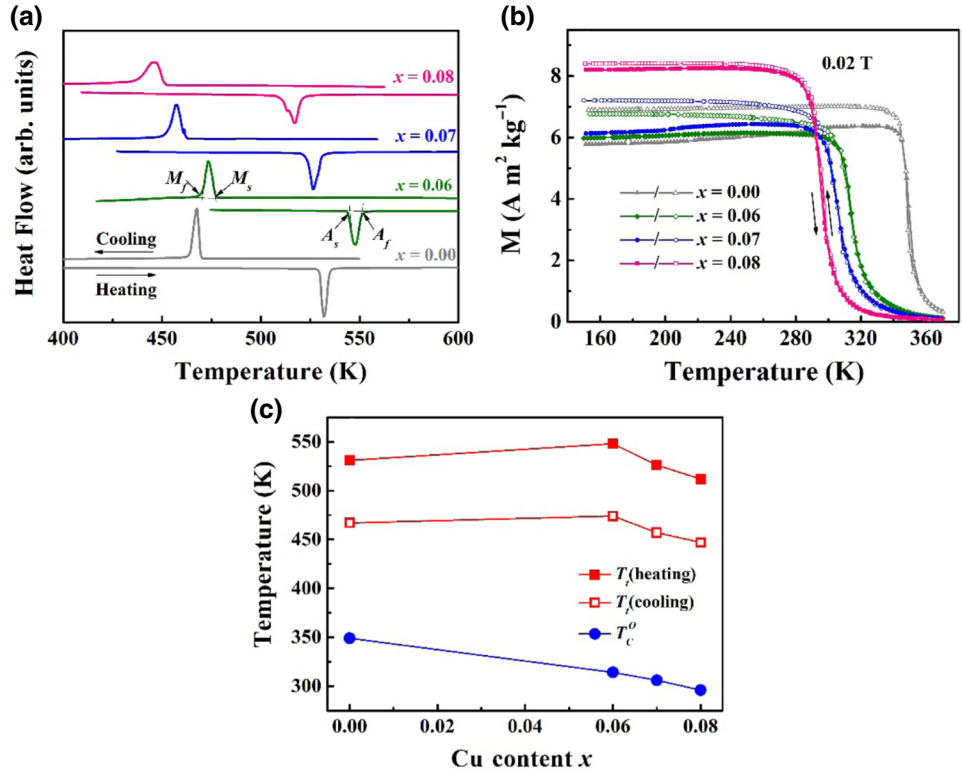

FIG. 3. (a) DSC curves and (b) *M-T* curves in a field of 0.02 T in heating and cooling processes for $MnCo_{1-x}Cu_xGe$ alloys. (c) Evolution of characteristic temperatures, T_t(heating), T_t(cooling), and T_C^O, as a function of Cu content.

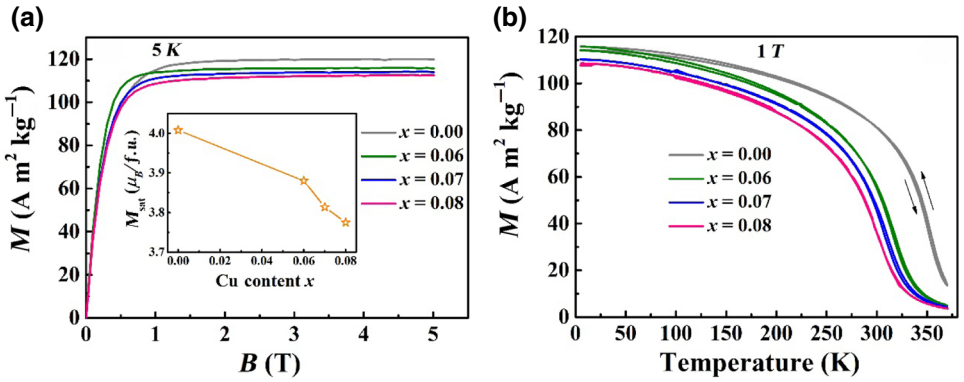

FIG. 4. (a) *M-B* curves at 5 K for $MnCo_{1-x}Cu_xGe$ alloys. Inset shows the saturation magnetization as a function of Cu content. (b) *M-T* curves in a field of 1 T for $MnCo_{1-x}Cu_xGe$ alloys.

lattice parameters and atomic site occupancies are performed on the reported experimental lattice parameters of MnCoGe [28]. Additionally, the interatomic exchange interaction calculations are performed using the Korringa-Kohn-Rostoker Green function method within the spin-polarized scalar-relativistic formalism (SPR KKR) [29]. The potential is treated within the atomic sphere approximation (ASA). The lattice parameters of orthorhombic phases are linearly interpolated from the experimental values of MnCoGe and $MnCo_{0.92}Cu_{0.08}Ge$, as shown in Table I. 100 and 1000 k points are chosen for self-consistent field and exchange-interaction calculation, respectively (details are shown in the Supplemental Material [30]).

III. RESULTS

A. Structural information

Figure 2 shows the XRD patterns of $MnCo_{1-x}Cu_xGe$ ($x = 0.00$, 0.06, 0.07, and 0.08) alloys at room temperature. All samples crystallize in the TiNiSi-type orthorhombic structures (*Pnma*, space group 62), which indicate that the structural transition occurs above room temperature. A small amount of the hexagonal structure, less than 4%, can be also obtained, which may result from the effect of residual stress during the grinding process [31]. According to the site-occupation principle in MnMX alloys [32], the Cu atom would occupy the 4c site of the Co atom. The lattice parameters and site occupation determined from the Rietveld refinement are listed in Table I. Evidently, an increase in lattice parameters a and c can be observed, while parameter b shrinks with the introduction of Cu. Consequently, the unit-cell volume expands from 160.89 Å^3 ($x = 0.00$) to 162.14 Å^3 ($x = 0.08$) due to the larger atomic radius of the Cu atom compared with that of Co.

B. Thermal and magnetic properties

To confirm T_t, DSC curves of $MnCo_{1-x}Cu_xGe$ ($x = 0.00$, 0.06, 0.07, 0.08) alloys are shown in Fig. 3(a). The large exothermic-endothermic peaks, with an obvious thermal hysteresis (ΔT_{hys}), correspond to the martensitic-austenitic transitions in MnMX-based alloys. The temperatures marked as, M_s, M_f, A_s, and A_f denote the start and finish points of the martensitic transition and austenitic transition, respectively. With increasing Cu content, T_t [defined as $T_t = (M_s + M_f)/2$ or $(A_s + A_f)/2$] first increases and then decreases. For the sample with $x \leq 0.08$, T_t remains in a relatively high-temperature range above room temperature, which suggests that the first-order structural transition is insensitive to the introduction of Cu onto the Co site. In Fig. 3(b), the thermomagnetic (*M-T*) curves clearly show the typical continuous PM-FM–type magnetic transition with negligible hysteresis below T_t. In comparison, the magnetic transition temperature, T_C^O, decreases

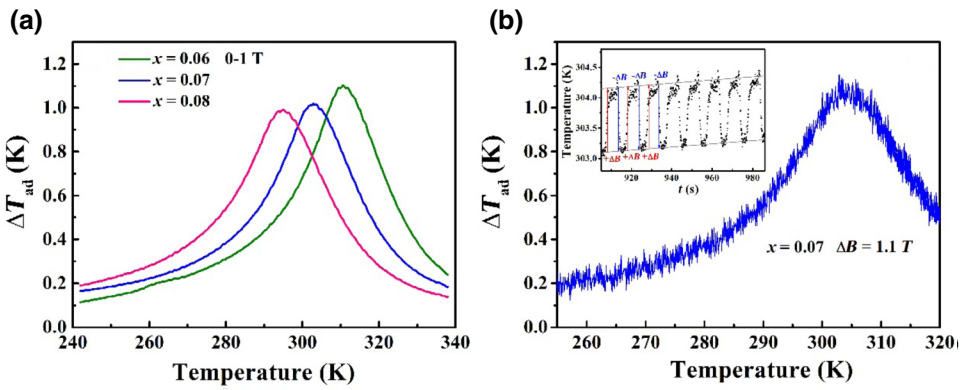

FIG. 5. (a) Temperature dependence of ΔT_{ad} for a field change of 0–1 T in $MnCo_{1-x}Cu_xGe$ ($x = 0.06$, 0.07, and 0.08) alloys. (b) Direct measurement of ΔT_{ad} in the temperature sweeping mode for the sample with $x = 0.07$ for $\Delta B = 1.1$ T. Inset shows data for temperature versus time signal around T_C^O during direct ΔT_{ad} measurements.

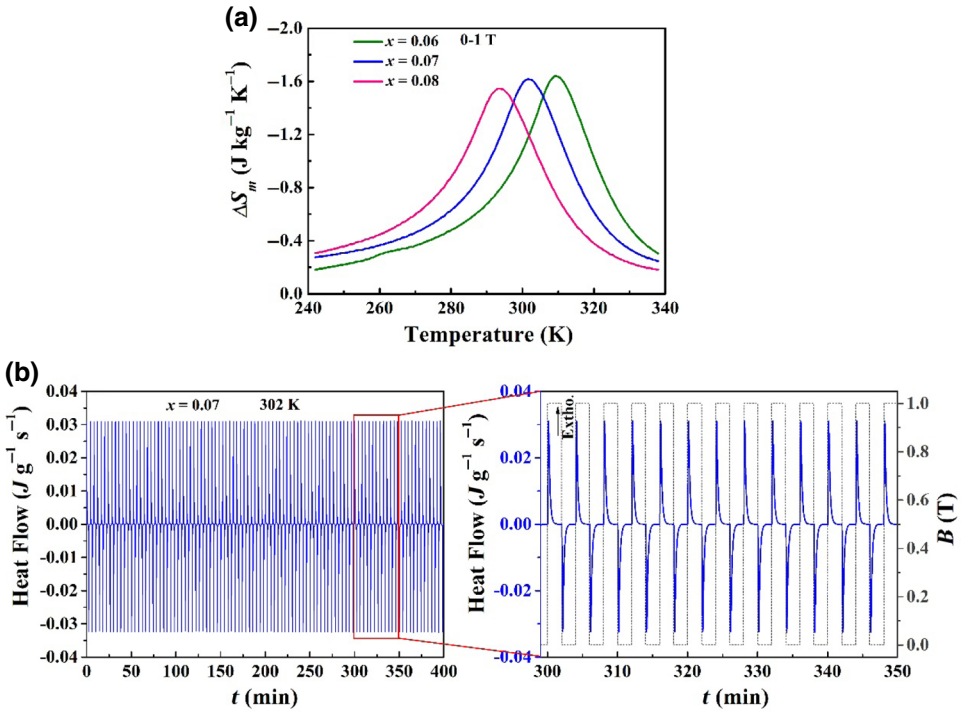

FIG. 6. (a) Temperature dependence of ΔS_m for a field change of 0–1 T for the $MnCo_{1-x}Cu_xGe$ ($x = 0.06$, 0.07, and 0.08) alloys. (b) Heat flow for 100 cyclic magnetic fields of 0–1 T for the sample with $x = 0.07$ at 302 K.

monotonously with increasing Cu content and can be tuned to room temperature, as shown in Fig. 3(c).

Due to the change of T_t and T_C^O, the samples of $x \leq 0.08$, possessing an orthorhombic structure, have a large saturation magnetization (M_{sat}), with values above 110 Am^2/kg (3.75 μ_B/f.u.), as shown in the magnetization (M-B) curves at 5 K in Fig. 4(a). This is because structural distortion during the martensitic transition brings about a larger Mn-Mn separation in the orthorhombic structure, which leads to narrower 3d band widths and a larger exchange splitting between the majority and minority bands [33]. A slight reduction in M_{sat} is attributed to the substitution of magnetic Co by nonmagnetic Cu. Therefore, benefiting from the above optimization, a considerable magnetization change during the room-temperature magnetic transition under 1 T is achieved, as shown in Fig. 4(b).

C. Magnetocaloric performance

The most straightforward assessment of MCE, ΔT_{ad}, as a function of temperature is derived from calorimetric measurements in a magnetic field. As shown in Fig. 5(a), ΔT_{ad} values of 1.1, 1.0, and 1.0 K under a field change of 0–1 T can be achieved for samples with $x = 0.06$, 0.07 and 0.08, respectively. Due to the negligible thermal hysteresis during the transition, the obtained value of ΔT_{ad} is expected to be reversible. Direct ΔT_{ad} measurements are also performed for the sample with $x = 0.07$. During measurements, the temperature sweeping mode with cyclic magnetic fields is adopted. As shown in Fig. 5(b), the largest ΔT_{ad} of about 1.1 K is achieved for $\Delta B = 1.1$ T, which is reversible during field oscillations.

Besides ΔT_{ad}, another important parameter, ΔS_m, is also derived from calorimetric measurements in a magnetic field upon cooling. The maximum values are about 1.6, 1.5, and 1.5 $Jkg^{-1}\,K^{-1}$ for samples $x = 0.06$, 0.07, and 0.08, respectively, as shown in Fig. 6(a). To evaluate the reversibility of this entropy change, direct measurements of the entropy change for a field change of 1 T are shown in Fig. 6(b). The exothermic (endothermic) peak upon applying (removing) the field represents the conventional MCE. During 100 cycles in this study, the peak height is almost unchanged, which demonstrates that the phase transitions possess good reversibility and stability. The calculated ΔS_m value is consistent with the indirect value (not shown here).

IV. DISCUSSION

Here, the SOMT is achieved in the $MnCo_{1-x}Cu_xGe$ system by stabilizing the structural transition at high temperature and decreasing T_C^O to room temperature (confirmation of the order of the magnetic transition is shown in the Supplemental Material [30]), which is beneficial to obtain the room-temperature, low-field, and reversible MCE. As reported in the literature, the stoichiometric MnCoGe alloy is very sensitive to the introduction of substitutional elements, resulting in a rapid decrease in T_t by increasing substitution concentrations [7,12,16,34–39]. In contrast, T_t exhibits a nonmonotonic change by Cu doping for Co in this work. To gain an insight into the origin of this distinct experimental result, the ELF of a supercell

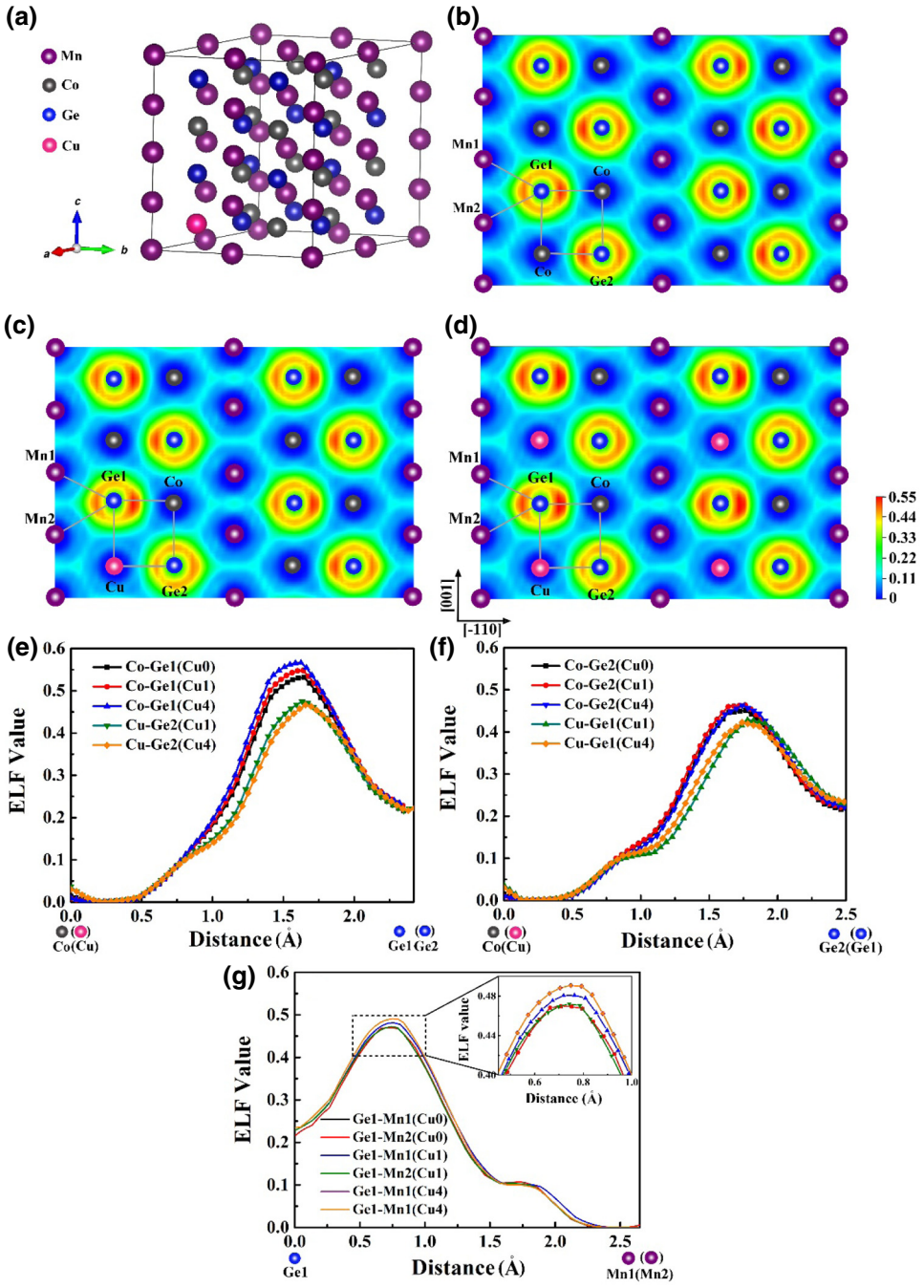

FIG. 7. (a) Crystalline structure of the $MnCo_{0.9375}Cu_{0.0625}Ge$ supercell for the hexagonal phase. ELF of (110) planes in (b) MnCoGe, (c) $MnCo_{0.9375}Cu_{0.0625}Ge$, and (d) $MnCo_{0.75}Cu_{0.25}Ge$. Variation of ELF value between nearest-neighbor (e) Co or Cu and Ge atoms along [−110] direction, (f) Co or Cu and Ge atoms along [001] direction, and (g) Mn-Ge atoms.

with hexagonal structure, as shown in Fig. 7(a), is calculated for compositions MnCoGe, $MnCo_{0.9375}Cu_{0.0625}Ge$, and $MnCo_{0.75}Cu_{0.25}Ge$ (denoted as Cu0, Cu1, and Cu4, respectively) to evaluate the bond's nature and change in bond strength [14,40]. The crystalline structures of supercells Cu0 and Cu4 and the selection of the configuration of Cu1 are shown in the Supplemental Material [30]. Figures 7(b)–7(d) show the ELF results of (110) plane of the hexagonal structure of Cu0, Cu1 and Cu4, respectively. Electrons in the stoichiometric MnCoGe alloy are mainly localized around the Ge atoms, especially between the nearest-neighbor Co and Ge along the [−110] direction, and the maximum ELF value is about 0.55. These results give rise to two important conclusions. First, the formed weak covalentlike bonding between Co and Ge, as the framework, supports stabilization of the hexagonal phase. Second, electron pairing as a result of bonding reduces the magnetic moments in both Co and Ge atoms [41]. When Cu is introduced into the Co site, the electrons' localized strength between different atoms changes, as shown in Figs. 7(c) and 7(d). Specifically, the extracted ELF values between nearest-neighbor Co-Ge, Cu-Ge, and

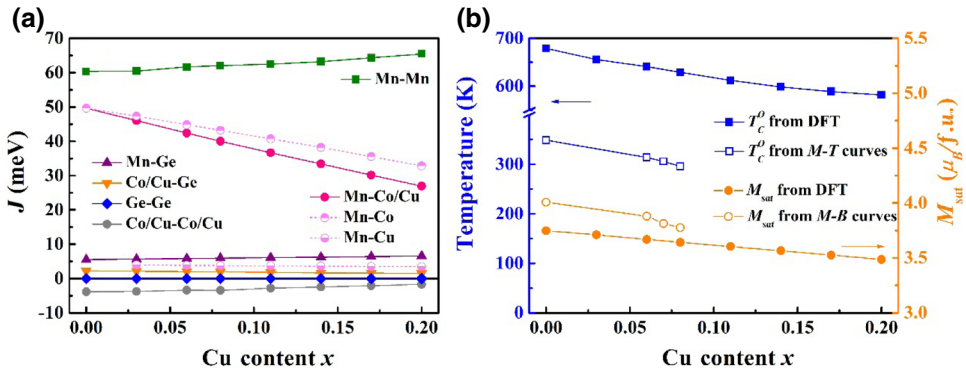

FIG. 8. (a) Calculated exchange coupling constants between the atoms in $MnCo_{1-x}Cu_xGe$ alloys as a function of the Cu content. (b) Estimated Curie temperature and saturation magnetization of the orthorhombic phase from DFT calculations and magnetic measurements in $MnCo_{1-x}Cu_xGe$ alloys, respectively.

Mn-Ge in Figs. 7(e)–7(g) can reflect the change more clearly. Obviously, the introduction of the Cu atom enhances the electrons' localized character between the Co and Ge atoms along the [−110] direction, while fewer electrons are localized between Cu and Ge atoms along the [−110] direction. This relatively weak localization between Cu and Ge atoms can also be observed along the [001] direction. In addition, the ELF value increases slightly between Mn and Ge atoms with increasing Cu content, indicating an enhanced localized character. Consequently, the strength of the covalentlike bonding from *p-d* hybridization is weakened between Cu and Ge and is mainly enhanced between Co and Ge, which destabilizes and stabilizes the hexagonal structure, respectively. The competition of both leads to the nonmonotonic change of T_t.

The exchange coupling constants J between different atoms in the $MnCo_{1-x}Cu_xGe$ alloys with an orthorhombic structure are calculated in Fig. 8(a). In stoichiometric MnCoGe, the Mn-Mn and Mn-Co exchange interactions are positive and strong. This is reasonable, as the magnetic moment is large for Mn atoms (3 μ_B) and small for Co atoms (0.8 μ_B) [42]. Considering other interactions, the strength is weak and negligible. Notably, Co-Co is found to show an antiferromagnetic coupling. When nonmagnetic Cu is introduced into the Co site, the strength of the Mn-Mn interaction slightly increases, while the Mn-Co interaction gradually deceases. Mn-Cu exhibits a weak ferromagnetic coupling and, with increasing Cu content, the statistical weight of this exchange interaction increases. Details of the evolution of J with the distance are shown in the Supplemental Material [30]. Based on the strength of J, the Curie temperature is estimated using mean-field theory from the following equation [43,44]:

$$T_C = \frac{2}{3k_B} J_{\max}, \tag{1}$$

where $J_{\max}$ is the largest eigenvalue of the matrix of the exchange coupling between the atoms. This matrix has the following form:

$$\begin{pmatrix} \sum J_{\mathrm{Mn-Mn}} & \sum J_{\mathrm{Mn-Co/Cu}} & \sum J_{\mathrm{Mn-Ge}} \\ \sum J_{\mathrm{Co/Cu-Mn}} & \sum J_{\mathrm{Co/Cu-Co/Cu}} & \sum J_{\mathrm{Co/Cu-Ge}} \\ \sum J_{\mathrm{Ge-Mn}} & \sum J_{\mathrm{Ge-Co/Cu}} & \sum J_{\mathrm{Ge-Ge}} \end{pmatrix}. \tag{2}$$

As shown in Fig. 8(b), T_C^O estimated from the DFT calculations decreases monotonously with increasing Cu contents, which is consistent with the experimental behavior. In addition, the calculated value of M_{sat} is in good agreement with the value from *M-B* curves given in Fig. 4(a). The specific atomic and total magnetic moments of orthorhombic and hexagonal structures calculated from SPR KKR or VASP are shown and compared in the Supplemental Material [30]. Evidently, the calculated value of T_C^O is overestimated, which is widely reported for the mean-field method [45,46]. Therefore, DFT calculations suggest that both the weak interactions between the Mn and Cu atoms and the decrease of Mn-Co interactions are responsible for the reduction of T_C^O.

In the MnMX family, the intrinsic ΔT_{hys} is the origin of irreversibility of MCE during the first-order magnetic transition. For instance, the $Mn_{0.92}CoCu_{0.08}Ge$ alloy, possessing a typical PM-FM–type MST, shows only a reversible ΔT_{ad} of about 0.35 K under a field change of 0–1.1 T due to the large ΔT_{hys} of 15 K. However, even the hysteresis can be reduced, such as 10 K in $Mn_{0.7}Fe_{0.3}NiGe_{0.7}Si_{0.3}$ alloy and 4–6 K in the $Mn_{0.9}Fe_{0.2}Ni_{0.9}Ge_{1-x}Si_x$ system [18,47], so the reversible ΔT_{ad} is also limited under low-field variation. This is because the low sensitivity of the MST to the magnetic field aggravates the irreversibility of the MCE under a low-field change in the MnMX system, which is always neglected. Details on the reversible ΔT_{ad} under low-field changes are discussed in the Supplemental Material [30]. In comparison, the $MnCo_{1-x}Cu_xGe$ alloy studied in this work shows a larger

low-field and reversible MCE around room temperature by taking advantage of SOMT without hysteresis. When compared with other magnetocaloric materials, the measured value of ΔT_{ad} for the sample with $x = 0.07$ is comparable with the reversible values in the Ni-Mn-based Heusler alloys, Mn_2Sb-based alloys, (Hf, Ta)Fe_2-based alloys, and $Tb_x(Dy_{0.5}Ho_{0.5})_{1-x}Co_2$ compounds at their first-order magnetic transitions under the same field change [48–51]. Additionally, we also need to point out that the reversible MCE in this work is weaker than that in the famous $(Mn, Fe)_2(P, Si)$-and $La(Fe, Si)_{13}$-based alloys and pure Gd. Therefore, it is necessary to increase magnetization of the orthorhombic phase and replace expensive geranium to further improve the magnetocaloric performance in the future.

V. CONCLUSIONS

We realize a reversible low-field magnetocaloric effect at room temperature in the Mn*MX* family. The introduction of Cu onto the Co site of MnCoGe results in stabilization of the martensitic transition at high temperatures and a decrease of T_C^O in the MnCoGe alloy. Thus, a reversible ΔT_{ad} of about 1 K under a field change of 0–1 T is achieved during the second-order magnetic transition of the orthorhombic phase. Moreover, DFT calculations are carried out to investigate the physical origin of the experimental results. The ELF analysis reveals that the strength of the covalentlike bonding between Cu and Ge is weakened and is enhanced between Co and Ge, which leads to a nonmonotonic change of T_t. The reduction in T_C^O is ascribed to a weak coupling between Mn and Cu atoms and a decrease in Mn-Co interactions. Our work deepens our understanding of the MnCoGe system and further develops its magnetocaloric performance towards practical applications.

ACKNOWLEDGMENTS

The authors would like to thank A. J. E. Lefering, B. Zwart, and K. Goubitz for their technical help. This work is sponsored by the NWO in the Domain Applied and Engineering Sciences (AES) Programme and the National Natural Science Foundation of China (Grants No. 11974184, No. 51601092, No. 51571121, and No. U1832191). J.L. gratefully acknowledges financial support from the China Scholarship Council.

[1] V. K. Pecharsky and K. A. Gschneidner, Jr., Giant Magnetocaloric Effect in $Gd_5(Si_2Ge_2)$, Phys. Rev. Lett. **78**, 4494 (1997).

[2] E. Brück, Developments in magnetocaloric refrigeration, J. Phys. D: Appl. Phys. **38**, R381 (2005).

[3] J. Liu, T. Gottschall, K. P. Skokov, J. D. Moore, and O. Gutfleisch, Giant magnetocaloric effect driven by structural transition, Nat. Mater. **11**, 620 (2012).

[4] T. Gottschall, K. P. Skokov, F. Scheibel, M. Acet, M. Ghorbani Zavareh, Y. Skourski, J. Wosnitza, M. Farle, and O. Gutfleisch, Dynamical Effects of the Martensitic Transition in Magnetocaloric Heusler Alloys From Direct ΔT_{ad} Measurements Under Different Magnetic-Field-Sweep Rates, Phys. Rev. Appl. **5**, 024013 (2016).

[5] O. Gutfleisch, M. A. Willard, E. Brück, C. H. Chen, S. G. Sankar, and J. P. Liu, Magnetic materials and devices for the 21st century: stronger, lighter, and more energy efficient, Adv. Mater. **23**, 821 (2011).

[6] V. Franco, J. S. Blázquez, J. J. Ipus, J. Y. Law, L. M. Moreno-Ramírez, and A. Conde, Magnetocaloric effect: From materials research to refrigeration devices, Prog. Mater. Sci. **93**, 112 (2017).

[7] N. T. Trung, L. Zhang, L. Caron, K. H. J. Buschow, and E. Brück, Giant magnetocaloric effects by tailoring the phase transitions, Appl. Phys. Lett. **6**, 172504 (2010).

[8] E. K. Liu, H. G. Zhang, G. Z. Xu, X. M. Zhang, R. S. Ma, W. H. Wang, J. L. Chen, H. W. Zhang, G. H. Wu, L. Feng, and X. X. Zhang, Giant magnetocaloric effect in isostructural MnNiGe-CoNiGe system by establishing a curie-temperature window, Appl. Phys. Lett. **102**, 122405 (2013).

[9] J. Liu, Y. Y. Gong, G. Z. Xu, G. Peng, I. A. Shah, N. ul Hassan, and F. Xu, Realization of magnetostructural coupling by modifying structural transitions in MnNiSi-CoNiGe system with a wide curie-temperature window, Sci. Rep. **6**, 23386 (2016).

[10] C. L. Zhang, D. H. Wang, Q. Q. Cao, Z. D. Han, H. C. Xuan, and Y. W. Du, Magnetostructural phase transition and magnetocaloric effect in off-stoichiometric $Mn_{1.9-x}Ni_xGe$ alloys, Appl. Phys. Lett. **93**, 122505 (2008).

[11] E. K. Liu, W. Zhu, L. Feng, J. L. Chen, W. H. Wang, G. H. Wu, H. Y. Liu, F. B. Meng, H. Z. Luo, and Y. X. Li, Vacancy-tuned paramagnetic/ferromagnetic martensitic transformation in Mn-poor $Mn_{1-x}CoGe$ alloys, EPL **9**, 17003 (2010).

[12] L. Caron, N. T. Trung, and E. Brück, Pressure-tuned magnetocaloric effect in $Mn_{0.93}Cr_{0.07}CoGe$, Phys. Rev. B **84**, 020414(R) (2011).

[13] T. Samanta, D. L. Lepkowski, A. U. Saleheen, A. Shankar, J. Prestigiacomo, I. Dubenko, A. Quetz, I. W. H. Oswald, G. T. McCandless, J. Y. Chan, P. W. Adams, D. P. Young, N. Ali, and S. Stadler, Hydrostatic pressure-induced modifications of structural transitions lead to large enhancements of magnetocaloric effects in MnNiSi-based systems, Phys. Rev. B **91**, 020401(R) (2015).

[14] E. K. Liu, W. H. Wang, L. Feng, W. Zhu, G. J. Li, J. L. Chen, H. W. Zhang, G. H. Wu, C. B. Jiang, H. B. Xu, and F. de Boer, Stable magnetostructural coupling with tunable magnetoresponsive effects in hexagonal ferromagnets, Nat. Commun. **3**, 873 (2012).

[15] Z. Y. Wei, E. K. Liu, Y. Li, G. Z. Xu, X. M. Zhang, G. D. Liu, X. K. Xi, H. W. Zhang, W. H. Wang, G. H. Wu, and X. X. Zhang, Unprecedentedly wide curie-temperature windows as phase-transition design platform for tunable magneto-multifunctional materials, Adv. Electron. Mater. **1**, 1500076 (2015).

[16] S. C. Ma, Q. Ge, Y. F. Hu, L. Wang, K. Liu, Q. Z. Jiang, D. H. Wang, C. C. Hu, H. B. Huang, G. P. Cao, Z. C. Zhong, and Y. W. Du, Driving higher magnetic field sensitivity of the martensitic transformation in MnCoGe ferromagnet, Appl. Phys. Lett. **111**, 192406 (2017).

[17] D. Kasimov, J. Liu, Y. Y. Gong, G. Z. Xu, F. Xu, and G. W. Lu, Realization of magnetostructural coupling in a high temperature region in $Mn_{0.85}Co_{0.3}Ni_{0.85}Si_{1-x}Ga_x$ system, J. Alloys Compd. **733**, 15 (2018).

[18] J. Liu, Y. Y. Gong, Y. R. You, X. M. You, B. W. Huang, X. F. Miao, G. Z. Xu, F. Xu, and E. Brück, Giant reversible magnetocaloric effect in MnNiGe-based materials: Minimizing thermal hysteresis via crystallographic compatibility modulation, Acta Mater. **174**, 450 (2019).

[19] J. Liu, K. Skokova, and O. Gutfleisch, Magnetostructural transition and adiabatic temperature change in Mn-Co-Ge magnetic refrigerants, Scr. Mater. **66**, 642 (2012).

[20] A. Kitanovski, J. Tušek, U. Tomc, U. Plaznik, M. Ozbolt, and A. Poredoš, *Magnetocaloric Energy Conversion: From Theory to Applications, Green Energy and Technology* (Springer International Publishing, 2014).

[21] F. Scarpa, G. Tagliafico, and L. A. Tagliafico, A classification methodology applied to existing room temperature magnetic refrigerators up to the year 2014, Renew. Sust. Energ. Rev. **50**, 497 (2015).

[22] V. Johnson, Diffusionless orthorhombic to hexagonal transitions in ternary silicides and germanides, Inorg. Chem. **14**, 1117 (1975).

[23] S. Nizioł, A. Weselucha, W. Bażela, and A. Szytuła, Magnetic properties of the $Co_xNi_{1-x}MnGe$ system, Solid State Commun. **39**, 1081 (1981).

[24] T. Roisnel and J. Rodríquez-Carvajal, WinPLOTR: A windows tool for powder diffraction pattern analysis, Mater. Sci. Forum **378**, 118 (2001).

[25] G. Porcari, F. Cugini, S. Fabbrici, C. Pernechele, F. Albertini, M. Buzzi, M. Mangia, and M. Solzi, Convergence of direct and indirect methods in the magnetocaloric study of first order transformations: The case of Ni-Co-Mn-Ga heusler alloys, Phys. Rev. B **86**, 104432 (2012).

[26] F. Guillou, G. Porcari, H. Yibole, N. van Dijk, and E. Brück, Taming the first-order transition in giant magnetocaloric materials, Adv. Mater. **26**, 2671 (2014).

[27] G. Kresse and J. Furthmüller, Efficient iterative schemes for *ab initio* total-energy calculations using a plane-wave basis set, Phys. Rev. B **54**, 11169 (1996).

[28] T. Kanomata, H. Ishigaki, T. Suzuki, H. Yoshida, S. Abe, and T. Kaneko, Magneto-volume effect of $MnCo_{1-x}Ge$ ($0 \leq x \leq 0.2$), J. Magn. Magn. Mater. **140**, 131 (1995).

[29] H. Ebert, D. Ködderitzsch, and J. Minár, Calculating condensed matter properties using the KKR-green's function method—recent developments and applications, Rep. Prog. Phys. **74**, 096501 (2011).

[30] See the Supplemental Material at http://link.aps.org/supplemental/10.1103/PhysRevApplied.13.054003. Figure S1 shows the isothermal magnetization curves measured around T_C^O and the derived Arrott plot for the sample with $x = 0.07$. Figure S2 shows the magnetic entropy change and the exponent n for the sample with $x = 0.07$, to confirm the order of the thermomagnetic transition quantitively. Figure S3 presents the crystalline structures of the supercells of calculated Cu0 and Cu4. Figure S4 shows the possible configurations of Cu1. Figure S5 shows the distance dependence of the exchange interaction parameter, J, between atoms. Figures S6(a) and S6(b) show the temperature dependence of the magnetization and reversible ΔT_{ad} under 0–1.1 T for $Mn_{0.92}CoCu_{0.08}Ge$. Figure S6(c) shows the temperature dependence of ΔT_{ad} from DSC in field measurements for $Mn_{0.9}Fe_{0.2}Ni_{0.9}Ge_{0.9}Si_{0.1}$. Figure S6(d) compares the largest reversible ΔT_{ad} during the magnetostructural transition in some typical Ni-Mn-based Heusler alloys. Table S1 shows the k-points tests during the SCF and the exchange-interaction process for composition $x = 0$ and 0.08. Table S2 presents the magnetic moments of hexagonal Cu0, Cu1, and Cu4 calculated from VASP. Table S3 shows the magnetic moments of orthorhombic MnCoGe from VASP and orthorhombic $MnCo_{1-x}Cu_xGe$ from SPR KKR.

[31] S. Singh, P. Kushwaha, F. Scheibel, H. P. Liermann, S. R. Barman, M. Acet, C. Felser, and D. Pandey, Residual stress induced stabilization of martensite phase and its effect on the magnetostructural transition in Mn-rich Ni-Mn-In/Ga magnetic shape memory alloys, Phys. Rev. B **92**, 020105 (2015).

[32] A. Szytuła, A. T. Pędziwiatr, Z. Tomkowicz, and W. Bażela, Crystal and magnetic structure of CoMnGe, CoFeGe, FeMnGe and NiFeGe, J. Magn. Magn. Mater. **25**, 176 (1981).

[33] J. T. Wang, D. S. Wang, C. F. Chen, O. Nashima, T. Kanomata, H. Mizuseki, and Y. Kawazoe, Vacancy induced structural and magnetic transition in $MnCo_{1-x}Ge$, Appl. Phys. Lett. **89**, 262504 (2006).

[34] N. T. Trung, V. Biharie, L. Zhang, L. Caron, K. H. J. Buschow, and E. Brück, From single- to double-first-order magnetic phase transition in magnetocaloric $Mn_{1-x}Cr_xCoGe$ compounds, Appl. Phys. Lett. **96**, 162507 (2010).

[35] T. Samanta, I. Dubenko, A. Quetz, S. Stadler, and N. Ali, Giant magnetocaloric effects near room temperature in $Mn_{1-x}Cu_xCoGe$, Appl. Phys. Lett. **101**, 242405 (2012).

[36] S. C. Ma, Y. X. Zheng, H. C. Xuan, L. J. Shen, Q. Q. Cao, D. H. Wang, Z. C. Zhong, and Y. W. Du, Large room temperature magnetocaloric effect with negligible magnetic hysteresis losses in $Mn_{1-x}V_xCoGe$ alloys, J. Magn. Magn. Mater. **324**, 135 (2012).

[37] T. Samanta, I. Dubenko, A. Quetz, S. Stadler, and N. Ali, Large magnetocaloric effects over a wide temperature range in $MnCo_{1-x}Zn_xGe$, J. Appl. Phys. **113**, 17A922 (2013).

[38] G. J. Li, E. K. Liu, H. G. Zhang, Y. J. Zhang, J. L. Chen, W. H. Wang, H. W. Zhang, G. H. Wu, and S. Y. Yu, Phase diagram, ferromagnetic martensitic transformation and magnetoresponsive properties of Fe-doped MnCoGe alloys, J. Magn. Magn. Mater. **332**, 146 (2013).

[39] L. F. Bao, F. X. Hu, R. R. Wu, J. Wang, L. Chen, J. R. Sun, B. G. Shen, L. Li, B. Zhang, and X. X. Zhang, Evolution of magnetostructural transition and magnetocaloric effect with Al doping in $MnCoGe_{1-x}Al_x$ compounds, J. Phys. D: Appl. Phys. **50**, 464005 (2017).

[40] B. Silvi and A. Savin, Classification of chemical bonds based on topological analysis of electron localization functions, Nature **371**, 683 (1994).

[41] J. Frenkel, On the correct formulation of pauli's exclusion principle, Nature **125**, 235 (1930).

[42] S. Nizioł, A. Bombik, W. Baz˚ela, A. Szytuła, and D. Fruchart, Crystal and magnetic structure of $Co_xNi_{1-x}MnGe$ system, J. Magn. Magn. Mater. **27**, 281 (1982).

[43] E. Şaşioğlu, L. M. Sandratskii, and P. Bruno, First-principles calculation of the intersublattice exchange interactions and curie temperatures of the full heusler alloys Ni_2MnX (X=Ga,In,Sn,Sb), Phys. Rev. B **70**, 024427 (2004).

[44] S. Sinjay, L. Caron, S. W. D'Souza, T. Fichtner, G. Porcari, S. Fabbrici, C. Shekhar, S. Chadov, M. Solzi, and C. Felser, Large magnetization and reversible magnetocaloric effect at the second-order magnetic transition in heusler materials, Adv. Mater. **28**, 3321 (2016).

[45] I. Turek, J. Kudrnovský, V. Drchal, and P. Bruno, Exchange interactions, spin waves, and transition temperatures in itinerant magnets, Phil. Mag. **86**, 1713 (2006).

[46] S. Ener, M. Fries, F. Hammerath, I. Opahle, E. Simon, P. Fritsch, S. Wurmehl, H. Zhang, and O. Gutfleisch, Magnetic and magnetocaloric properties of the $Co_{2-x}Mn_xB$ system by experiment and density functional theory, Acta Mater. **165**, 270 (2019).

[47] A. Taubel, T. Gottschall, M. Fries, T. Faske, K. P. Skokov, and O. Gutfleisch, Influence of magnetic field, chemical pressure and hydrostatic pressure on the structural and magnetocaloric properties of the Mn-Ni-Ge system, J. Phys. D: Appl. Phys. **50**, 464005 (2017).

[48] J. Liu, X. M. You, B. W. Huang, I. Batashev, M. Maschek, Y. Y. Gong, X. F. Miao, F. Xu, N. van Dijk, and E. Brück, Reversible low-field magnetocaloric effect in Ni-Mn-In-based heusler alloys, Phys. Rev. Mater. **3**, 084409 (2019).

[49] A. Tekgül, M. Acet, F. Scheibel, M. Farle, and N. Ünal, The reversibility of the inverse magnetocaloric effect in $Mn_{2-x}Cr_xSb_{0.95}Ga_{0.05}$, Acta Mater. **124**, 93 (2017).

[50] L. V. B. Diopab, J. Kastilabc, O. Isnardab, Z. Arnoldc, and J. Kamaradc, Magnetic and magnetocaloric properties of itinerant-electron system $Hf_{1-x}Ta_xFe_2$ ($x = 0.125$ and 0.175), J. Alloys Compd. **627**, 446 (2015).

[51] V. B. Chzhan, I. S. Tereshina, A. Yu. Karpenkov, and E. A. Tereshina-Chitrova, Persistent values of magnetocaloric effect in the multicomponent laves phase compounds with varied composition, Acta Mater. **154**, 303 (2018).